Wide-Field Vibrational Phase Imaging

Pascal Berto,[1] David Gachet,[1,2] Pierre Bon,[1] Serge Monneret,[1] and Hervé Rigneault[1,*]

[1]*Institut Fresnel, CNRS UMR 7249, Aix-Marseille Université, Ecole Centrale Marseille, Campus de Saint Jérôme, F-13397 Marseille, France*

[2]*CINaM, CNRS UMR 7325, Aix-Marseille Université, Campus de Luminy, F-13288 Marseille, France*

(Received 5 March 2012; published 28 August 2012)

We propose and implement a wide-field microscopy method to retrieve the real and imaginary part of a field emitted by coherent and resonant molecular scatterers. The technique is based on wave-front sensing and does not require the use of any reference beam. We exemplify its ability in wide-field coherent anti-Stokes Raman scattering imaging and retrieve the complex anti-Stokes field while spectrally scanning a molecular vibrational resonance. This approach gives access to the background-free Raman spectrum of the targeted molecular bond.

DOI: 10.1103/PhysRevLett.109.093902 PACS numbers: 42.65.Dr, 42.25.Hz, 78.47.nj, 87.64.mn

Retrieving the weak complex field emitted by coherent molecular scatterers is always a difficult task in the optical domain as it generally relies on performing interference between the field emitted by the molecule and a reference field. By contrast, wave-front sensors give access to both the field amplitude and phase without the use of a reference beam as they are able to determine the wave-front curvature at any spatial location in the measured area. Nevertheless, wave-front sensors are usually not compatible with molecular spectroscopy and microscopy as they exhibit a poor spatial resolution and are mostly implemented on cameras with sensitivities that are not compatible with weak field measurement. Molecular spectroscopy and its extension to microscopy would greatly benefit from a pure physical and simple complex field retrieval technique as both the real and imaginary parts of the scattered field are necessary to fully describe the light-matter interaction. This is indeed the case in coherent Raman spectroscopy (CRS) that aims at capturing the vibrational signature of molecular scatterers. CRS implemented in microscopy is nowadays a mature field aiming at providing to the biologist a label-free molecular imaging technique [1]. Whereas most of the efforts have been concentrated to point-scanning approaches, wide-field CRS has received less attention although it has several benefits for applications. Wide-field coherent anti-Stokes Raman scattering (CARS) microscopy has the ability to image a large field of view in a single shot scheme as demonstrated by pioneer works in the field [2]. Both phase-matching [3] and non–phase-matching [4,5] illumination conditions can be used in wide-field CARS.

As in point-scanning CARS, wide-field CARS is not background-free and a CARS image remains visible when the frequency difference between the incoming pump and Stokes beams is tuned far from the vibrational resonance. This is intrinsically due to the CARS intensity detection scheme that mixes both the real and the imaginary parts of the nonlinear susceptibility $\chi^{(3)}(\omega_{as}) = \mathrm{Re}[\chi^{(3)}(\omega_{as})] + i\mathrm{Im}[\chi^{(3)}(\omega_{as})]$ together with the additional significant contribution of nonresonant four-wave mixing to $\mathrm{Re}[\chi^{(3)}(\omega_{as})]$. Various approaches have been implemented in CARS to circumvent the undesirable effects of this nonresonant background, including Epi [6], polarization sensitive [7], and time-resolved [8] detection modes that mostly filter out the nonresonant nonlinear susceptibility. Optical heterodyne detection schemes have also been proposed [9–12] and are of particular interest because they have the ability to retrieve $\mathrm{Im}[\chi^{(3)}(\omega_{as})]$, a quantity that is proportional to the spontaneous Raman signal [13]. Wide-field CARS holography has been recently proposed by mixing the generated CARS signal with a reference beam coming from an optical parametric oscillator [14] or a nonlinear layer set in front of the specimen [15]. Wide-field second-harmonic generation holography has also been reported using a reference beam generated in a frequency doubling crystal [16]. Such heterodyne schemes are not artifact-free as they rely on stabilizing an interferometer with long arms and dealing with the scattering of the reference beam through the sample itself. To circumvent these effects the ''cascaded phase-preserving chain'' implemented in CARS [11] is particularly interesting because the phase of the excitation fields that have crossed the sample is actually measured and subtracted from the phase of the CARS signal to correct *de facto* changes in refractive index in the sample, phase curvature over the field of view, and interferometric instabilities in order to retrieve the vibrational phase. The latter approach requires three incoming beams and can be implemented in point-scanning microscopy.

In this work we propose and demonstrate a completely different scheme to measure the phase of the CARS signal in a wide-field configuration and with two quasicollinear incoming pump and Stokes beams.

This so called ''vibrational phase'' is due to the phase shift (or time lag) associated with the vibrational resonance and is directly linked to $\mathrm{Im}[\chi^{(3)}(\omega_{as})]$. Using an optimized

wave-front sensor located in the image plane, we map here the phase of the CARS signal generated by polystyrene beads when spectrally scanning a molecular resonance around 1000 cm^{-1} in a collinear CARS excitation configuration. Far from resonance, the wide-field CARS signal is mostly due to the surrounding nonresonant background and its phase only reflects the refraction from the sample. This "refractive phase" $\varphi_{\mathrm{REFRACT}}$ constitutes a phase offset. On resonance, the wave front experiences an additional vibrational phase φ_{CARS} that is the very signature of the targeted vibrational bond (Fig. 1).

In order to get more insight into the proposed vibrational phase measurement, we have performed numerical calculations based on a three-dimensional vectorial model that takes into account the focusing of the incoming fields and the CARS signal generation by a set of discrete induced nonlinear (polarization) dipoles that mesh the bead sample in three dimensions [17,18]. This model has been further developed to include the CARS field propagation down to the image plane. We consider here a $2, 4 \times 2, 4 \times 20\ \mu m^3$ rectangular bulk volume along the x, y, and z directions filled with a nonresonant medium with nonlinear susceptibility $\chi^{(3)NR}_{\mathrm{bulk}}$. In the defined bulk volume is located a 1 μm diameter bead whose nonlinear susceptibility is $\chi^{(3)NR}_{\mathrm{bead}} + \chi^{(3)R}_{\mathrm{bead}}$, with $\chi^{(3)R}_{\mathrm{bead}} = 2\chi^{(3)NR}_{\mathrm{bead}}$ and $\chi^{(3)NR}_{\mathrm{bead}} = \chi^{(3)NR}_{\mathrm{bulk}}$ as obtained from a fit to the experimental measured CARS spectra of a polystyrene bead embedded in an index matching oil. The weakly focused pump and Stokes beams ($NA_{\mathrm{excitation}} = 0.1$) propagate along the z axis and define an 8 μm diameter active CARS area. For the sake of simplicity and to understand how the vibrational phase acts on the CARS field, these simulations do not take into account the refractive index mismatch between the bead and its surrounding. We will see later that this is not detrimental as it can be experimentally achieved by performing an adequate wave-front subtraction to cancel out the refractive phase $\varphi_{\mathrm{REFRACT}}$. Figures 2(a) and 2(b) present simulated wide-field CARS images of the described sample

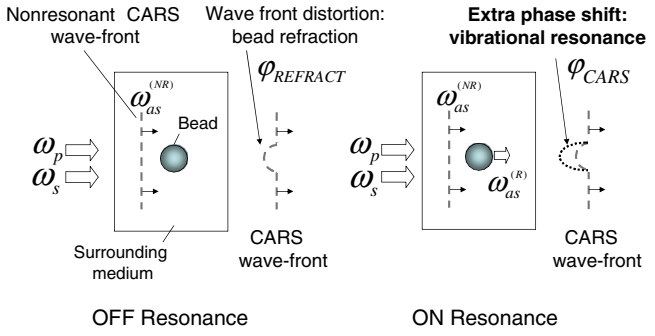

FIG. 1 (color online). Principle of the spatial phase alteration in wide-field CARS microscopy. Off resonance, the shape of the CARS wave front reflects the refractive index of the sample whereas on resonance an extra phase shift alters the wave-front shape.

obtained with a $NA_{\mathrm{collection}} = 0.8$ objective lens. In the intensity image [Fig. 2(a)], the bead is not visible due to the strong nonresonant contribution of the bulk medium. On the contrary, the phase image [Fig. 2(b)] clearly highlights the bead. In this case, the phase shift is found to be $|\varphi_{\mathrm{CARS}}| = 8°$. This weak phase shift, that is far from the 90° value expected on resonance, takes its origin in the nonresonant contribution to the total CARS field [Fig. 2(c)]: $E_{\mathrm{CARS}} \propto N_{NR}e^{i\varphi_{NR}} + N_R e^{i\varphi_R} = N_{NR} + N_R e^{-i(\pi/2)} = N_{NR} - iN_R$, where N_{NR} and N_R are the number of nonresonant and resonant scatterers in the active CARS volume, respectively. The phase shift $\varphi_{\mathrm{CARS}} = -\arctan\frac{N_R}{N_{NR}}$ of the CARS field scales inversely with the nonresonant contribution. To show the relevance of this simple analysis, we compare in Fig. 2(d) the phase shift φ_{CARS}, retrieved from the full vectorial simulation, with the above simple analytical formula.

To measure the phase of the CARS field, we have implemented a wide-field CARS imaging experiment in a quasicollinear geometry [Fig. 3(a)]. The pump (730 nm) and Stokes (780 nm) beams are generated by two synchronized mode locked Ti:Saph lasers (3 ps, 76 MHz) that overlap in space and time at the sample location [19]. This particular pair of wavelengths matches the 1000 cm^{-1} band of polystyrene. The two laser beams are weakly focused into the sample through an achromatic doublet ($f = 35$ mm, $NA = 0.1$) As such, they define a 9 μm diameter CARS interaction volume at the center of which is located a 3 μm diameter polystyrene bead (Sigma-Aldrich, $n \approx 1.6$). The bead is embedded in a

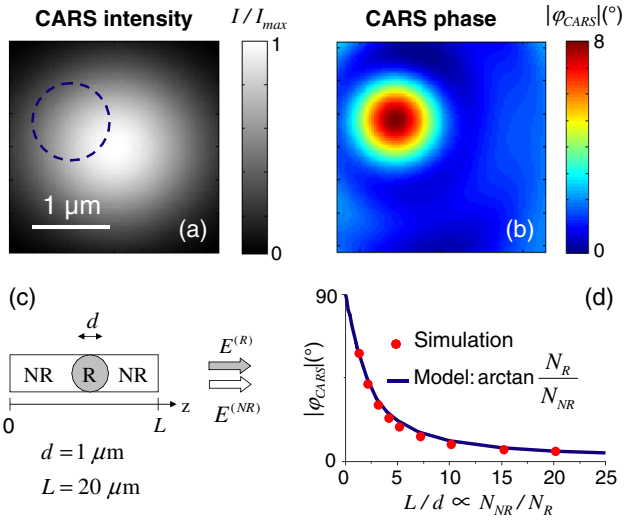

FIG. 2 (color online). Simulated CARS field in the image plane generated by a bead embedded in a nonresonant bulk medium. (a) CARS intensity with the overlaid bead location. (b) Phase φ_{CARS} of the CARS field. (c) Scheme of the interference between the resonant and nonresonant fields. (d) Vibrational phase φ_{CARS} versus the ratio of the nonresonant to the resonant field.

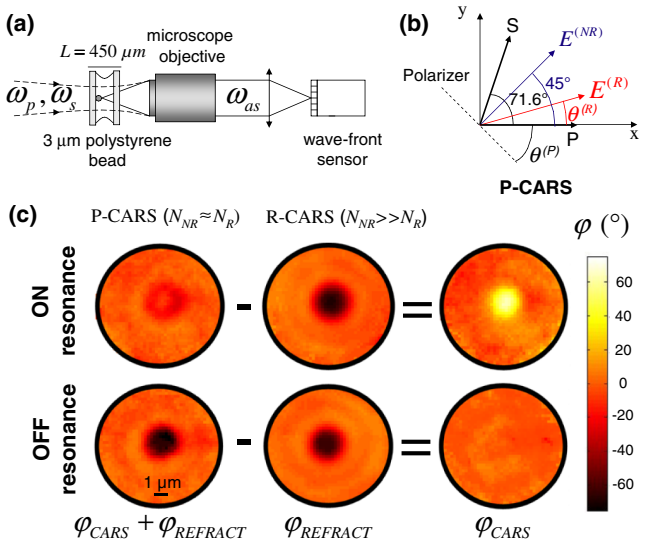

FIG. 3 (color online). (a) Experimental setup. (b) P-CARS scheme. (c) Spatial phase as measured by the wave-front sensor in the P-CARS and R-CARS schemes together with their difference off resonance (1058 cm^{-1}) and on resonance (1003 cm^{-1}). A vibrational phase shift of 60° is visible on resonance.

150 μm thick refraction index matching oil (Cargille Labs, Cargille Immersion Liquid Code OHZB, $n = 1.556$ at 25 °C) and sandwiched between two glass cover slips (thickness 150 μm). The anti-Stokes signal generated by the bead is imaged ($NA_{\text{collection}} = 0.65$) in the forward direction onto a two-dimensional wave-front sensor that can record both the amplitude and the phase of the anti-Stokes image field. This wave-front sensor is based on quadriwave lateral shearing interferometry (QWLSI) [20], a technique that does not require any mobile element and proves to be superior in terms of lateral resolution than Shack-Hartmann based sensors [21].

Briefly, QWLSI [22] uses a two-dimensional grating (modified Hartman mask) that generates four orders of diffraction which interfere on a CCD camera. If the incoming wave front is a plane wave, the interference pattern detected on the camera is a rectangular grid. Any local curvature in the wave front will distort the shape of this grid. The analysis of these distortions retrieves the phase gradient and the wave-front relative phase at any position in the image field. We have implemented a custom QWLSI sensor sensitive to the relatively weak anti-Stokes signal. It is based on an electron-multiplying CCD (EMCCD) camera and a grating initially designed for a commercially available QWLSI sensor (SID4Bio, Phasics, Palaiseau, France). Here, we use two different detection schemes sensitive to the wave-front curvature related either to the bead refractive phase φ_{REFRACT}, or to the vibrational phase at resonance φ_{CARS}. In the first, so called P-CARS scheme, we adopt the classical polarization CARS arrangement [23], where an angle of 71.6° is set between the pump and Stokes' linear polarization states. This configuration sets an angle of $\theta^{(NR)} = 45°$ between the CARS nonresonant background and the pump's linear polarization state [Fig. 3(b)]. Any Raman mode with depolarization ratio ρ_R gives rise to a resonant anti-Stokes field which linear polarization makes an angle $\theta^{(R)} = \arctan[\rho_R \tan(71.6°)]$ with the pump's polarization state. In the present experiment, $\rho_R \approx 0$ for the targeted 1000 cm^{-1} and 1030 cm^{-1} lines of polystyrene [24], setting $\theta^{(R)} \approx 0$. A polarizer, oriented in the vicinity of $\theta^{(P)} = -45°$ [Fig. 3(b)], permits us to suppress *most of* the nonresonant background. Fine tuning its angle subsequently adjusts the ratio $\frac{N_R}{N_{NR}}$ (and therefore the CARS phase shift φ_{CARS}—see [Fig. 2(d)]). In this P-CARS configuration, the total phase shift is thus given by $\varphi_{\text{CARS}} + \varphi_{\text{REFRACT}}$. In the second, so called R-CARS scheme, the same 71.6° relative angle is kept between the pump and Stokes beams' polarization while the anti-Stokes signal is now detected without polarizer. The weakly focused pump and Stokes beams define a CARS interaction volume far larger than the bead ($L/d > 100$—see [Fig. 2(c)]). Consequently, most of the CARS signal comes from the surrounding medium. A part of this strong nonresonant CARS signal is generated before the beam crosses the bead itself (Fig. 1). This specific signal imprints on the wave front a spatial phase shift φ_{REFRACT} solely due to the refractive index mismatch between the medium and the bead. The final subtraction of the two phase shifts measured in the P-CARS and R-CARS schemes gives access to the vibrational phase shift φ_{CARS}.

Our EMCCD-based QWLSI sensor can record phase and amplitude images of a 3 μm polystyrene bead within 100 ms and 40 s in the R-CARS and P-CARS schemes, respectively (on resonance, with 100 mW incoming pump and Stokes average powers).

Figure 3(c) shows the results of the P-CARS and the R-CARS spatial phase measurements together with their difference (average of 30 images). Far from the vibrational resonance (1058 cm^{-1}), the P-CARS and R-CARS phases are similar and are attributed to φ_{REFRACT} only. This is not the case on resonance (1000 cm^{-1}), where a clear φ_{CARS} is retrieved by the signal difference. The value of the vibrational phase $\varphi_{\text{CARS}} = 60°$ corresponds to the awaited $\frac{N_{NR}}{N_R} = 1.9$ [see Fig. 2(d)] as settled in the experiment. The positive value of φ_{CARS} is a consequence of the P-CARS projection on the polarizer and is further described in the Supplemental Material [25].

From φ_{CARS} and the P-CARS intensity I_{CARS}, it is easy to retrieve the real and imaginary parts $\sqrt{I_{\text{CARS}}}\cos(\varphi_{\text{CARS}})$ and $\sqrt{I_{\text{CARS}}}\sin(\varphi_{\text{CARS}})$ of the complex CARS field. They are proportional to the real and imaginary parts of the third order nonlinear susceptibility $\chi^{(3)}$, respectively. Figure 4 shows the evolution of the imaginary [Fig. 4(b)] and real [Fig. 4(c)] parts of the complex CARS field when the vibrational resonance is scanned from 950 cm^{-1} to 1100 cm^{-1} (open circles). On the same graph are plotted the theoretical

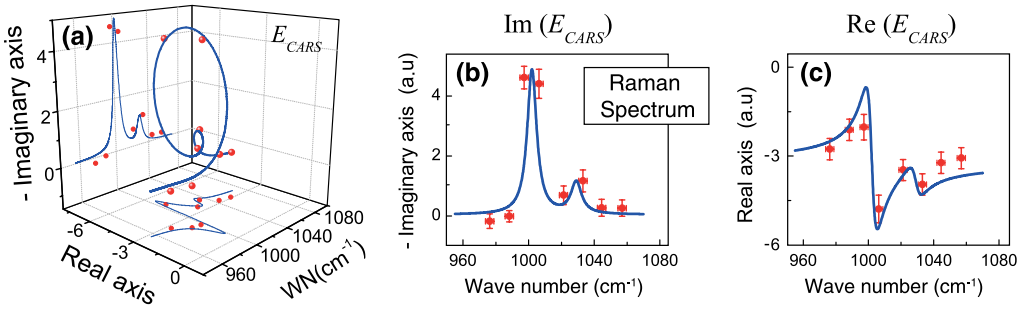

FIG. 4 (color online). Evolution of the complex CARS field when spectrally crossing a molecular resonance: measurements (red circles) and simulation (blue solid curves). (a) Three-dimensional representation, (b) imaginary part (proportional to the spontaneous Raman spectrum), and (c) real part.

curves (solid lines) expected from the spontaneous Raman spectrum of polystyrene and a ratio $N_R/N_{NR} = 1.9$. The real part adds up the dispersive line shape of the resonant contribution and a constant nonresonant contribution. On the other hand, the imaginary part follows the expected polystyrene Raman spectrum, with its two characteristic resonances at 1003 cm^{-1} and 1034 cm^{-1}. Interesting is the complex spectral volume representation of the data depicted in Fig. 4(a) where any molecular resonance defines a loop. These loops are here again the signature of the vibrational phase φ_{CARS}. This "molecular roller coaster," as described in Ref. [26], is the very signature of the resonance and contains the information carried by both the real and imaginary parts of the field.

Similar to P-CARS spectroscopy, in our P-CARS configuration the transmitted signal through the polarizer depends on the depolarization ratio of the probed Raman line. As a consequence, the recovered Raman spectra might have the amplitude of their peaks modulated as compared to spontaneous Raman spectra. However, this effect is only marginal when a specific vibrational mode is targeted as performed in CARS imaging applications. We note that the quasicollinear geometry used here is interesting for the vibrational phase measurement because it (i) fulfills CARS phase matching, (ii) generates a strong nonresonant background required in R-CARS to retrieve $\varphi_{\mathrm{REFRACT}}$, and (iii) produces a nonresonant background area in the recorded image which is necessary for the sensor to adequately reconstruct the absolute phase map. As a consequence, the field of view must be larger than the CARS targeted specimen and the available laser power will fix its maximal dimensions.

In conclusion, we have proposed and implemented a wide-field microscopy method to retrieve the real and imaginary parts of a field emitted by coherent molecular scatterers. The technique is based solely on a wide-field wave-front analysis. We illustrate the technique in the CARS context and measure the vibrational phase that is imprinted on the wave front when crossing the Raman molecular resonance. Spectrally, this vibrational phase fully maps the resonance in the complex plane, the projection of which, along the imaginary axis, is the background-free Raman spectrum. We note that the proposed method is purely physical and does not require any phase retrieval algorithm [27,28]. Spatially, this vibrational phase is compatible with three-dimensional CARS imaging that can be realized by the digital propagation of the complex anti-Stokes field in a way similar to what is done in digital holography [14]. The presented approach is not limited to nonlinear processes and applies to any process exhibiting both coherent and resonant features (resonant scattering in atoms, molecules, and dielectric or metallic micro- or nanoresonators, for instance); it has the advantage over classical wide-field heterodyne techniques to be self-referenced and to not require the use of any reference beam.

We thank Dan Oron and Esben Andresen for fruitful discussions. We thank Phasics SA [29] and especially Lucie de Laulanié for their assistance in the development of the EMCCD-based wave-front sensor. We acknowledge financial support from the French research agency (ANR), The "Fond unique interministeriel," the CNRS, the Région Provence-Alpes-Côte d'Azur, and the European Union (grant CARSExplorer FP7 Health and COST MP603 MicroCARS).

*Corresponding author.
herve.rigneault@fresnel.fr

[1] W. Min, C. W. Freudiger, S. Lu, and X. S. Xie, Annu. Rev. Phys. Chem. **62**, 507 (2011).
[2] C. Heinrich, S. Bernet, and M. Ritsch-Marte, Appl. Phys. Lett. **84**, 816 (2004).
[3] C. Heinrich, A. Hofer, A. Ritsch, C. Ciardi, S. Bernet, and M. Ritsch-Marte, Opt. Express **16**, 2699 (2008).
[4] I. Toytman, K. Cohn, T. Smith, D. Simanovskii, and D. Palanker, Opt. Lett. **32**, 1941 (2007).
[5] M. Lei, M. Winterhalder, R. Selm, and A. Zumbusch, J. Biomed. Opt. **16**, 021102 (2011).
[6] A. Volkmer, J.-X. Cheng, and X. S. Xie, Phys. Rev. Lett. **87**, 023901 (2001).
[7] J.-X. Cheng, L. D. Book, and X. S. Xie, Opt. Lett. **26**, 1341 (2001).

[8] A. Volkmer, L. D. Book, and X. S. Xie, Appl. Phys. Lett. **80**, 1505 (2002).
[9] N. Dudovich, D. Oron, and Y. Silberberg, Nature (London) **418**, 512 (2002).
[10] E. O. Potma, C. L. Evans, and X. S. Xie, Opt. Lett. **31**, 241 (2006).
[11] M. Jurna, J. P. Korterik, C. Otto, J. L. Herek, and H. L. Offerhaus, Phys. Rev. Lett. **103**, 043905 (2009).
[12] D. Gachet, S. Brustlein, and H. Rigneault, Phys. Rev. Lett. **104**, 213905 (2010).
[13] R. W. Hellwarth, Prog. Quantum Electron. **5**, 1 (1977).
[14] K. Shi, H. Li, Q. Xu, D. Psaltis, and Z. Liu, Phys. Rev. Lett. **104**, 093902 (2010).
[15] Q. Xu, K. Shi, H. Li, K. Choi, R. Horisaki, D. Brady, D. Psaltis, and Z. Liu, Opt. Express **18**, 8213 (2010).
[16] E. Shaffer, C. Moratal, P. Magistretti, P. Marquet, and C. Depeursinge, Opt. Lett. **35**, 4102 (2010).
[17] J.-X. Cheng, A. Volkmer, and X. S. Xie, J. Opt. Soc. Am. B **19**, 1363 (2002).
[18] D. Gachet, F. Billard, and H. Rigneault, J. Opt. Soc. Am. B **25**, 1655 (2008).
[19] N. Djaker, D. Gachet, N. Sandeau, P. F. Lenne, and H. Rigneault, Appl. Opt. **45**, 7005 (2006).
[20] P. Bon, G. Maucort, B. Wattellier, and S. Monneret, Opt. Express **17**, 13080 (2009).
[21] J. Primot, Opt. Commun. **222**, 81 (2003).
[22] J. Primot and L. Sogno, J. Opt. Soc. Am. A **12**, 2679 (1995).
[23] J. L. Oudar, R. W. Smith, and Y. R. Shen, Appl. Phys. Lett. **34**, 758 (1979).
[24] W. M. Sears, J. L. Hunt, and J. R. Stevens, J. Chem. Phys. **77**, 1639 (1982).
[25] See Supplemental Material at http://link.aps.org/supplemental/10.1103/PhysRevLett.109.093902 for the phase analysis of the CARS field in the P-CARS scheme.
[26] M. Jurna, E. T. Garbacik, J. P. Korterik, J. L. Herek, C. Otto, and H. L. Offerhaus, Anal. Chem. **82**, 7656 (2010).
[27] E. M. Vartiainen, H. A. Rinia, M. Muller, and M. Bonn, Opt. Express **14**, 3622 (2006).
[28] Y. Liu, Y. J. Lee, and M. T. Cicerone, Opt. Lett. **34**, 1363 (2009).
[29] B. Wattelier, Phasics, http://www.phasicscorp.com.